JOURNAL OF GUIDANCE, CONTROL, AND DYNAMICS
Vol. 33, No. 6, November–December 2010

Dynamical Systems Analysis of Planetary Flybys and Approach: Planar Europa Orbiter

Rodney L. Anderson*
University of Colorado at Boulder, Boulder, Colorado 80309-0431
and
Martin W. Lo†
Jet Propulsion Laboratory, California Institute of Technology, Pasadena, California 91109

DOI: 10.2514/1.45060

In this analysis, the relationship between a planar Europa Orbiter trajectory and the invariant manifolds of resonant periodic orbits is studied. An understanding of this trajectory with its large impulsive maneuvers should provide basic tools that can be extended to cases that approximate low thrust with many small maneuvers. This study therefore represents a step in understanding low-thrust trajectories. Unstable resonant orbits are computed along with their invariant manifolds in order to examine the resonance transitions that the planar Europa Orbiter trajectory travels through. The stable manifold of a Lyapunov orbit at the L_2 libration point is used to show why a 5:6 resonance is necessary at this energy for capture around Europa.

I. Introduction

THIS research seeks to reexamine Galilean moon tours using dynamical systems techniques in the context of the planar circular restricted three-body problem with the goal of developing techniques that will be applicable to such tours as well as to similar low-thrust scenarios. The fact that dynamical systems methods may be applied to low-thrust trajectories was suggested by the work of Bollt and Meiss [1]. They considered a trajectory from the Earth to the moon using the recurrence properties of chaotic dynamics in the Earth–moon–spacecraft three-body problem. One of the features of deterministic chaos is that only a very weak force is required to effect large changes in the orbits, a fact first observed by Poincaré [2]. The *weak force* immediately suggests that a low-thrust engine may be used. However, an issue with their work is that it took 2.05 years to reach the moon from a high Earth orbit ($\sim$60,000 km circular radius above Earth). Schroer and Ott [3] reduced the transfer time to nine months, which is much more practical for actual space missions. They identified a sequence of unstable resonant periodic orbits using a Poincaré section of the dynamical region between the Earth and the moon. By targeting the invariant manifolds of these orbits, they were able to significantly reduce the transfer time. They specifically noted that their targeting method is very relevant to low-thrust trajectory design. None of these papers, however, noted the role of the invariant manifolds of Lyapunov orbits in the final ballistic capture by the moon depicted in their figures. These two seminal works suggest that resonant orbits and libration orbits both play a part in low-thrust trajectory optimization in this energy regime.

The use of resonant orbits for mission design is, of course, not new. In almost all of the intricate multiple planetary flyby trajectories, some form of resonance is used. However, in these instances, the fundamental model of the solar system is a series of coupled two-body problems. The spacecraft trajectory is modeled as segments of conic arcs around the sun, planet, or satellite of the moment. These arcs are produced either by Lambert's theorem or by B-plane analysis of hyperbolic flybys. Resonance is used to find conic arcs that provide repeated flybys of a body to either reduce or increase the orbital energy in the two-body sense. These arcs are then patched together to form a pseudo trajectory. Using differential correction (parallel shooting), this approximate solution may be transformed into a fully integrated solution with complex dynamical models, such as the Jet Propulsion Laboratory (JPL) ephemeris of the solar system [4].

One of the reasons for using resonant flybys is that the resulting trajectories have much lower propulsion (ΔV) cost. Physically, this is explained by the exchange of momentum between the spacecraft and the planetary body it flies by. Heuristically, the energy reduction is often credited to N-body effects. Recently, Strange and Longuski [5] and Okutsu et al. [6] introduced the Tisserand criterion in the design of flyby trajectories. This, of course, is the inclusion of three-body dynamics into the problem, because Tisserand's criterion is an approximation of the Jacobi constant expressed in convenient orbital element form. The success of this method suggests that three-body effects are important in the flyby problem and can be used to reduce the orbital energy required. However, dynamically, this is still unsatisfying because it leaves many questions unanswered. For example, why do certain resonant flybys provide greater energy savings than others? How do ballistic captures occur?

Tisserand originally derived his criterion for the study of comet motions. This suggests that we examine the motion of comets in the solar system for insight into these questions. In some sense, comets travel on the quintessential low-thrust trajectory due to their natural outgassing. It is well known that many comets are in resonant orbits with the planets. The Jupiter family of orbits are known to transition between the 3:2 and 2:3 resonances frequently, sometimes with temporary captures around Jupiter for several revolutions. Gehrels 3, Oterma, and Helin–Roman–Crockett are examples of such comets [7,8]. A more detailed explanation of resonance will follow in the Background section.

Belbruno and Marsden [9] proposed that the weak stability boundary may be used to explain the comet resonance transitions. Lo and Ross [10] suggested that the invariant manifolds of libration orbits play a role in the resonance transitions. This suggestion was verified theoretically by Koon et al. [7], showing that the invariant manifolds of the 3:2 and 2:3 resonant orbits near Jupiter and the Lyapunov orbits around Jupiter's L_1 and L_2 provide the low-energy resonant transfer and temporary capture mechanism for Jupiter

Presented as Paper 2004-5305 at the AIAA/AAS Astrodynamics Specialist Conference, Providence, RI, 16–29 August 2004; received 25 April 2009; revision received 15 October 2009; accepted for publication 2 November 2009.

*Research Associate, Colorado Center for Astrodynamics Research, Aerospace Engineering Sciences, Campus Box 431 UCB. Member AIAA.

†Member of Technical Staff, High Capability Computing and Modeling Group, 4800 Oak Grove Drive. Member AIAA.

comets. Howell et al. [8] numerically verified this transition and capture mechanism by comparing the orbits of several Jupiter family comets (mentioned earlier) with the segments of invariant manifolds of libration orbits around Jupiter's L_1 and L_2 computed in the full JPL ephemeris model. Lo et al. [11] examined the relationship of ballistic flyby trajectories to the invariant manifolds of resonant orbits. This analysis was extended to lay the groundwork for the current paper in a series of papers by Lo et al. [11], Anderson and Lo [12], Anderson [13], and Lo et al. [14].

All of the ingredients are now available to analyze the resonant flybys and ballistic capture of the planar Europa Orbiter (PEO) trajectory. The PEO trajectory as it is used in this paper is a planar version of a spatial Europa Orbiter trajectory designed at JPL in 1999 [15]. In the following analysis, the process of finding the unstable resonant orbits for the 3:4 and 5:6 resonances will be discussed along with their characteristics. The PEO trajectory will then be compared to the unstable resonant orbits and their invariant manifolds at each energy level or Jacobi constant. An L_2 Lyapunov orbit and the resonant orbits will then be used to analyze the Europa approach.

This paper lays the foundation for the ultimate goal of designing a low-thrust trajectory for a mission like the proposed JIMO (Jupiter Icy Moons Orbiter, cancelled in 2005) or similar Petit Grand Tours. Some of these same techniques have already been used to examine a low-thrust trajectory in the Jovian system [13]. Once the tools, both theoretical and numerical, for constructing and analyzing the PEO trajectory are developed, the low-thrust trajectory problem can be approached as follows. The next step involves constructing a pseudo low-thrust trajectory using multiple small impulsive thrusts using the invariant manifolds as guides. The pseudo orbit can be used as an initial guess trajectory for input into optimization programs such as Mystic [16]. Such initial guesses would be expected to greatly reduce the computation time for a converged optimal low-thrust trajectory with complex dynamical models. Moreover, the ΔV estimates provided by the pseudo orbits should be sufficiently accurate compared to those produced by the integrated optimized solutions. These pseudo orbits would serve the same role for low-thrust trajectories in the three-body regime as patched conic solutions provide for planetary flybys with impulsive maneuvers in the two-body regime.

II. Background

A. Europa Orbiter Trajectory

The current analysis uses a planar version of an impulsive Europa Orbiter trajectory as a first step in understanding the resonance transitions to the Europa approach and capture segments of low-thrust trajectories such as those designed for the proposed JIMO mission. The PEO trajectory is similar to the proposed JIMO trajectory in that it is designed for the Galilean system, it undergoes energy or velocity changes, and it ultimately must go into orbit around Europa. Given these similarities, the techniques developed for analyzing the PEO should be readily extended to low-thrust trajectories for Petit Grand Tours. A differential corrector [17,18] in JPL's Libration Point Mission Design Tool (LTool) is used to transfer the original Europa Orbiter trajectory [15] from the case using the full ephemerides to the planar circular restricted three-body problem (PCRTBP) while preserving the topological and ΔV characteristics of this trajectory. The portion of the trajectory traveling from Ganymede to Europa was selected as the focus of this study.

The design of the original Europa Orbiter trajectory using a model including the full ephemerides of the Galilean moons has been described in detail by Johannesen and D'Amario [15] in addition to others [6,19,20]. This trajectory was developed primarily using two-body conic techniques for the tour design with inclusion of three-body perturbations in the integration for the final Europa approach. The design of the approach to Europa consisted of modifying an initial guess for the Europa orbit insertion (EOI) ΔV and the orbit around Europa and then integrating backward until it matched with the rest of the tour. Of particular interest to this research is the fact that the Europa Orbiter design uses the last portion of a sequence of resonances developed by Yen at JPL (as described in [15]) as a good compromise between time and ΔV for a Europa approach. This sequence terminates with the 3:4 and 5:6 resonant flybys of Europa. The other Europa Orbiter scenarios also target a 5:6 resonance as the last flyby before EOI. It was also observed that third-body perturbations ultimately allowed the spacecraft to loosely capture around Europa, resulting in a smaller EOI ΔV than would be expected from a conic analysis.

B. Circular Restricted Three-Body Problem

The circular restricted three-body problem (CRTBP) is the primary model used in this study. Szebehely [21] or Roy [22] may be referred to for detailed descriptions of this model, but a brief summary is given here. In the CRTBP, two bodies, typically referred to collectively as the primaries, are assumed to rotate about their center of mass in circular orbits, and the objective is to describe the motion of a third infinitesimal mass placed in this system. If the infinitesimal mass is restricted to the plane of motion of the two primaries, the problem is called the planar CRTBP. In formulating the equations of motion for the infinitesimal mass, the required quantities are usually normalized and made dimensionless so that the mass of the smaller body (the secondary) is μ, and the larger body (the primary) has mass $1-\mu$. The distance between the two bodies becomes one with the primary located on a rotating x axis at $x_1 = -\mu$ and the secondary at $x_2 = 1-\mu$. The dimensionless time corresponds to the angle between the x axis of the rotating frame (defined so that the x axis always passes through the two bodies) and the x axis of the inertial frame. The period of the rotating system becomes 2π. Both the mean motion and the gravitational constant are one. Using this notation, the equations of motion for the infinitesimal mass in the rotating system may be written as

$$\ddot{x} - 2\dot{y} = x - (1-\mu)\frac{x-x_1}{r_1^3} - \mu\frac{x-x_2}{r_2^3}$$

$$\ddot{y} + 2\dot{x} = \left(1 - \frac{(1-\mu)}{r_1^3} - \frac{\mu}{r_2^3}\right)y \qquad \ddot{z} = -\left(\frac{(1-\mu)}{r_1^3} + \frac{\mu}{r_2^3}\right)z \tag{1}$$

Here the distances from the infinitesimal mass to the primary and secondary are r_1 and r_2, respectively. An energylike integral of motion exists in this model called the Jacobi constant, which varies when maneuvers are performed. It may be computed as

$$C = x^2 + y^2 + \frac{2(1-\mu)}{r_1} + \frac{2\mu}{r_2} - \dot{x}^2 - \dot{y}^2 \tag{2}$$

Finally, there are five equilibrium points in the problem (the Lagrange points) about which periodic orbits exist.

C. Periodic and Resonant Orbits

Periodic and resonant orbits are analyzed in detail in the following investigation, so it is helpful to discuss some of their characteristics and definitions. Many of the features of resonant periodic orbits are common to orbits in the two-body and three-body problem, so elliptical orbits in the two-body problem will be described first. In the two-body problem, any elliptical orbit is periodic in the inertial frame. A spacecraft on such an elliptical orbit will be periodic in the rotating frame defined by two primaries if the spacecraft travels around the larger primary p times for every q times the smaller primary travels around, given that $p, q \in \mathbb{N}$, the positive integers. The relationship between the resonant integers, mean motions, and periods of the spacecraft and the smaller primary may be written, respectively, as

$$\frac{p}{q} = \frac{n_p}{n_q} = \frac{T_q}{T_p} \tag{3}$$

The mean motion of the smaller primary n_q in the CRTBP is unity, so one criterion for the spacecraft to be periodic in the synodic frame is that $n_p = p/q$.

As mentioned previously, the dimensionless period of the smaller primary is 2π, and the configuration repeats itself after q revolutions of the smaller primary. So the period of the infinitesimal mass in the rotating frame is $2\pi q$. Note that in this paper, the form $p{:}q$ is used for

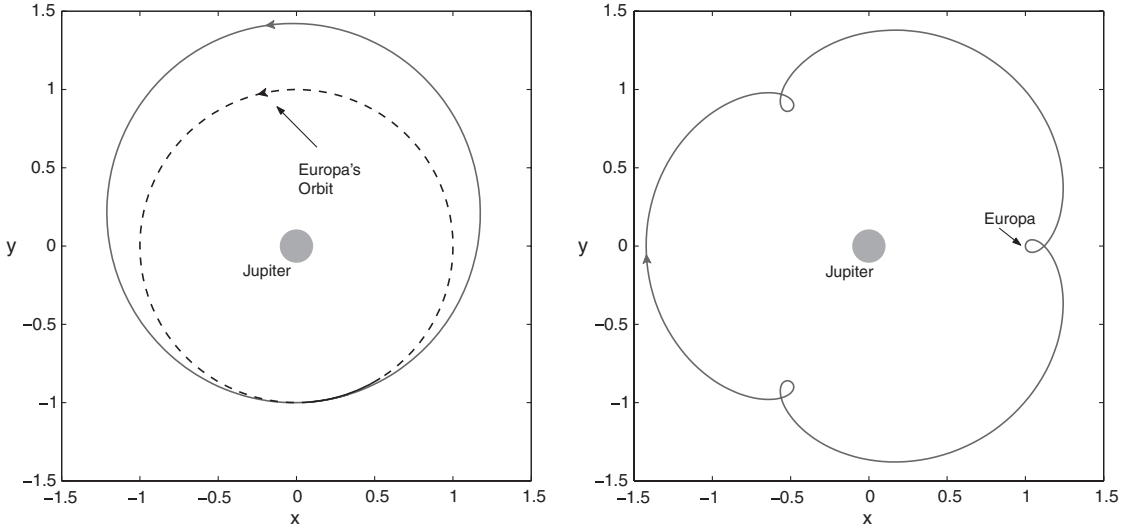

a) Inertial frame **b) Jupiter-Europa rotating frame**

Fig. 1 A 3:4 resonant elliptical orbit integrated in the two-body problem. The trajectory was determined so that its periapse was at Europa's radius, and it had a period equal to 4/3 that of Europa's period.

the resonances, which is equivalent to the ratio of the Europa period to the spacecraft period or spacecraft revolutions to Europa revolutions. This study will also primarily focus on exterior resonances, in which the period of the infinitesimal mass is greater than the period of the secondary. This focus makes sense, because the spacecraft is traveling from Ganymede, which is the next-farthest Galilean moon from Jupiter.

An example two-body elliptical orbit with a pericenter that intersects Europa's orbit in the Europa–Jupiter rotating frame is shown in Fig. 1 in both the inertial frame (Fig. 1a) and the rotating frame (Fig. 1b). Some of the graphical characteristics of resonant orbits that are also applicable to the three-body problem can be gleaned from this plot. There are three loops visible in the spacecraft trajectory, which correspond to the passage of the orbit through three pericenters. Note that, in general, the spacecraft is traveling in an opposite direction in the rotating frame than it is in the inertial frame. This characteristic is typical of an exterior orbit, since its period is larger than that of Europa, and it is generally traveling at a slower rate around Jupiter. The loops occur when the spacecraft approaches periapse, and it is momentarily traveling faster around Jupiter than Europa. In the rotating frame, it therefore appears to reverse its direction of motion.

In the two-body problem, the periods of the spacecraft and the smaller primary are related precisely by the resonant integers, but in the three-body problem this is no longer true. The definition used in this study follows that given by Murray and Dermott [23] for mean motion resonance, which is

$$pn_p \approx qn_q \tag{4}$$

In this case, if the system is integrated for q revolutions of the smaller primary $2\pi q$, the infinitesimal mass will generally not quite return to the original conditions as observed in the two-body problem. Usually, more time spent in the nonlinear regions near the Lagrange points will produce a greater difference from the two-body results. This definition may seem vague, so it is helpful to use Poincaré sections to search for *islands* corresponding to different resonances. Refer to Sec. III.E for an example Poincaré map with islands representing the resonances. For a more detailed explanation of these topics, see Murray and Dermott [23], Szebehely [21], or Barrabés and Gómez [24].

D. Poincaré Maps

Poincaré maps are useful for studying complicated systems because they bring out information that would otherwise be obscured [25]. To compute a Poincaré map for a system in $\mathbb{R}^n$, a *hypersurface* Σ or surface of section in $\mathbb{R}^{n-1}$ is placed transverse to the flow, as shown in Fig. 2. A trajectory intersecting the surface of section is integrated until it intersects the surface of section once again. The mapping is from the first intersection to the next intersection and so on. The points of the mapping may then be plotted using a number of different coordinates, although only some coordinates will result in visible structure. Given the planar CRTBP in $\mathbb{R}^4$, the surface of section is specified by fixing one of the coordinates in order to produce a surface in $\mathbb{R}^3$.

In this analysis, the surface of section is specified by $y = 0$ along the x axis opposite Europa (see Sec. III.E). The Jacobi constant is fixed for all the points in the Poincaré section, which means that the resulting surface of section is two-dimensional. So in a given Poincaré section, x and $\dot{x}$ are known, and $y = 0$. The magnitude of $\dot{y}$ can then be calculated in the planar problem from the Jacobi constant as

$$\dot{y} = \pm\sqrt{x^2 + y^2 + \frac{2(1-\mu)}{r_1} + \frac{2\mu}{r_2} - \dot{x}^2 - C} \tag{5}$$

As mentioned previously, resonant orbits and their invariant manifolds are of particular importance to this analysis, and their intersections with the surface of section are computed throughout this paper. It is also useful to compare these resonant orbits and invariant manifolds with the typical Poincaré section showing the stable quasi-periodic orbits and other structures at different resonances. For this analysis, only those points crossing the surface of section with a positive $\dot{y}$ are plotted, since only the resonant orbits crossing the $y = 0$ line with $-x$ values are of interest. The initial $\dot{x}$ is usually set equal to zero, but $\dot{x}$ is given a value of 0.05 when the main resonances of even order are of interest. See Murray and Dermott [23] for the rationale behind this technique. A Runge–Kutta–Fehlberg seventh-order integrator with step-size control is used to generate the Poincaré sections.

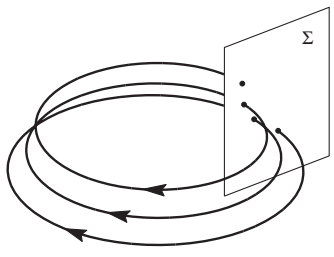

Fig. 2 Sample Poincaré map for a three-dimensional system.

Once the information for each intersection has been recorded, the question arises as to which quantities should be plotted. With y always zero, it is often useful to plot x and $\dot{x}$. Other quantities found to be helpful are the Delaunay variables [7] L and $\bar{g}$. L is the square root of the semimajor axis, and $\bar{g}$ is the argument of periapse relative to the rotating x axis. L was useful here in selecting a point with the desired initial conditions to aid in the location of unstable resonant orbits. Using the two-body equations and an estimation of the desired period of the orbit, a relationship between L and the resonance could be found according to

$$\frac{p}{q} = \frac{n_p}{n_q} = \frac{T_q}{T_p} = \frac{\sqrt{a_q^3/\mu_G}}{\sqrt{a_p^3/\mu_G}} \approx a_p^{-3/2} = L^{-3} \tag{6}$$

Here, μ_G is the gravitational parameter of the larger primary.

E. Single Shooting and Differential Correction

A single-shooting method was used to aid in finding the resonant orbits used in this study. The basic algorithm, described by Howell and Breakwell [26], was modified for the planar case. It uses the symmetry about the x axis in the CRTBP in order to search for periodic orbits. Given this symmetry, a trajectory that intersects the x axis twice with a velocity perpendicular to the x axis will be periodic. Using the algorithm for finding resonant orbits rather than halo orbits requires some additional modifications to the algorithm, since the first intersection with the x axis is not necessarily the desired intersection. The instability of the orbits used for this study puts a lower limit on the error of approximately 10^{-11} for the single-shooting technique [27].

The differential corrector implemented in JPL's LTool was used to aid in transferring trajectories between different models in this study. More detailed information related to the differential corrector may be found in Wilson [17] or Pernicka [18]. This differential corrector uses the state transition matrix in a two-level process to vary the states at given patch points in such a way as to produce a continuous trajectory. The version of the differential corrector in LTool has been written to allow the use of a variety of constraints that can be helpful in converging on a trajectory with specific characteristics.

F. Invariant Manifolds

A manifold may be most simply defined as an m-dimensional surface embedded in $\mathbb{R}^n$, which locally possesses the structure of $\mathbb{R}^m$ [25]. The term *invariant* indicates that a trajectory of a point on the manifold will remain on the manifold as time evolves. Invariant manifolds may be subdivided into stable and unstable manifolds. Simply speaking a stable manifold for a flow consists of those points that approach a limit set L as time moves forward toward infinity, while an unstable manifold consists of the points that approach the limit set as time moves backwards. A limit set for these purposes is a periodic orbit or an equilibrium point. More formally, the stable and unstable manifolds for a flow ϕ_t are as follows. The stable manifold $W^s(L)$ is the set of points x such that $\phi_t(x)$ approaches L as $t \to \infty$. The unstable manifold $W^u(L)$ is the set of points x such that $\phi_t(x)$ approaches L as $t \to -\infty$. See Parker and Chua [28] for more details.

In calculating the stable and unstable manifolds of a libration or resonant orbit, the fact that these orbits are periodic is used to discretize the continuous-time system and form a map. The Poincaré maps discussed earlier, where a surface Σ is constructed transverse to the flow at a particular point, are often used for this purpose. A similar concept is that of a stroboscopic map where the flow is observed at intervals equal to the period of the orbit [28]. In this case, the state transition matrix from the initial time t_o to the time after one period $(t_o + T)$ is referred to as the monodromy matrix and is designated by $\Phi(t_o + T, t_o)$. The algorithm for computing manifolds uses the fact that the eigenvector of the monodromy matrix corresponding to an eigenvalue greater (less) than one is in the direction of the local unstable (stable) manifold. To compute the manifold, an initial point corresponding to an offset of approximately 1.0×10^{-6} dimensionless units in the direction of the desired eigenvector is typically calculated [27]. For calculation of the unstable manifold, the trajectory is then integrated forward in time from the given point, and for the stable manifold, the trajectory is integrated backward in time.

G. Visualization of the Invariant Manifolds Relative to the PEO

Anderson [13] dealt with using a Poincaré surface of section to visualize the invariant manifolds of the resonant orbits relative to a trajectory. Computing the invariant manifolds for the unstable resonant orbits presents several difficulties that are not normally encountered when computing the invariant manifolds of libration orbits. Simply plotting these trajectories quickly becomes confusing, because they do not behave in the same manner as the trajectories on the invariant manifolds of libration orbits. The trajectories tend to travel to different resonances, but they stay in the same general vicinity of the original orbit in configuration space. One solution to this problem that aids in simplifying the comparison of the trajectories of interest with the invariant manifolds is the use of Poincaré sections. An interesting aspect of the surface of section chosen for this study is that it actually intersects the unstable orbit, which is different from the surface of sections typically chosen for libration orbits.

The calculation of the trajectories on the manifold is performed in the usual manner described above. This process involves taking offsets in phase space in the stable and unstable directions, and computing the trajectory from these offset states. These trajectories are not exactly on the manifold, but they follow or *shadow* the invariant manifold with varying degrees of accuracy, depending on the magnitude of the offset. The fact that the resonant orbits possess different characteristics from libration orbits made the selection of the offset uncertain. After a study of these offsets, a combination of offsets varying from approximately 1 km to 10 km was considered acceptable. The smaller offsets tended to require a long time to move away from the resonant orbit, so the larger offsets were used in order to help globalize the invariant manifolds more quickly. The fact that these manifolds computed at different offsets are generally connected and form continuous curves in the Poincaré section indicates that this method produces a good representation of the manifold. Another consideration in computing the Poincaré section is that the invariant manifolds grow and change shape between each successive pass through the surface of section. Using larger offsets bypasses some of these passes and more quickly computes the growth of the manifold. However, this introduces the risk of using too large of an offset and falling away from the manifold. Another factor is that the Poincaré section here actually contains the resonant orbit, unlike the case for libration orbits, where the Poincaré section is usually taken elsewhere. As a result, the Poincaré section for the resonant orbits contains just a slice out of the invariant manifolds. Furthermore, this slice contains points representing trajectories on the manifold that have just been computed as well as those that have almost completed one revolution. The continuity of the invariant manifolds in the Poincaré sections confirms that the use of relatively small offsets produces a faithful representation of the invariant manifolds.

III. Planar Europa Orbiter Trajectory

A. Transferring the Europa Orbiter Trajectory into the PCRTBP

This analysis focuses on the last portion of the Europa Orbiter trajectory from the first Europa flyby to EOI. This portion of the trajectory includes a transition between resonances via a gravity flyby as well as the final Europa approach scenario, both of which are

Table 1 Europa Orbiter trajectory events (for this segment)

Event	Epoch	Quantity	Value
Start (Europa flyby)	12 Sept. 2009, 1506 hrs	Europa alt	2010.0 km
ΔV_1	20 Sept. 2009, 0214 hrs	ΔV mag	118.4 m/s
Europa flyby	27 Sept. 2009, 0305 hrs	Europa alt	5392.0 km
ΔV_2	8 Oct. 2009, 0246 hrs	ΔV mag	91.6 m/s
EOI	19 Oct. 2009, 1329 hrs	ΔV mag	448.0 m/s

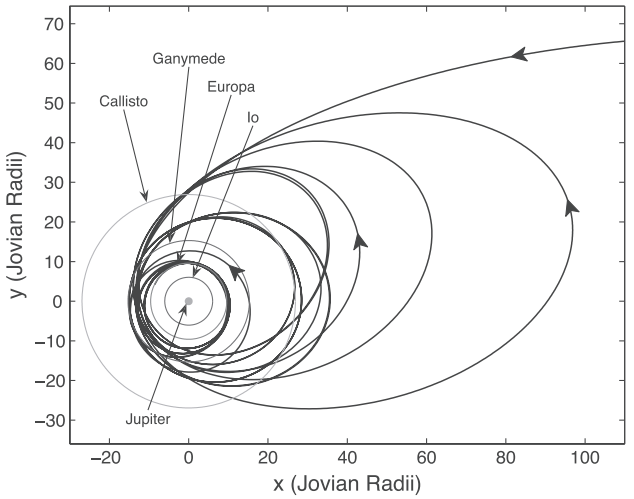

Fig. 3 The original Europa Orbiter trajectory in the inertial frame. The portion of interest here was the final approach to Europa.

key aspects to understanding trajectory design for a Galilean moon tour. The relevant events for this portion of the trajectory are listed in Table 1. Transferring the Europa Orbiter trajectory from the original version, which included all the ephemerides, to the planar version in the CRTBP involved a progressive series of changes in models with many intermediate steps.

As a first step in the transferal process, the trajectory, computed using the ephemerides of all of the bodies, was imported into LTool. The complete trajectory is shown in the inertial frame in Fig. 3. Again, the last portion of the trajectory approaching Europa is the focus of this current analysis. Several points, commonly referred to as patch points, were selected at regular intervals for use with the differential corrector. This initial trajectory was reconverged in LTool in order to take into account small differences in the ephemeris models. Unnecessary patch points were then eliminated by visual inspection in order to aid in the convergence during the next steps. Next, a crude continuation technique was used whereby the moons were removed from the model one at a time, and the differential corrector was used to recompute the trajectory after the removal of each moon until only Europa remained. This process worked well with the correct patch-point selection, although removing Io presented some difficulty and required modification of the patch points. For importation of the trajectory into the CRTBP, the patch points obtained in the previous model were placed into the CRTBP model all relative to Europa. This was necessary in order for the differential corrector to converge on a trajectory following the desired Europa approach. This approach proved successful in producing a trajectory that had the desired characteristics. The primary consideration in the differential correction process was retaining the topology and shape of the trajectory with the expectation that this would be most likely to preserve the dynamics that were of interest. More specifically, the objective was to retain the same resonances and similar ΔV locations between the two trajectories. This required careful selection of the patch points and constraints, since the differential corrector often tried to converge on a very different type of trajectory. The results can be observed by comparing the original trajectory in Fig. 4 with the spatial trajectory in the CRTBP in Fig. 5. Note that the distances in Fig. 4 are given in kilometers, whereas those in Fig. 5 are given in the usual CRTBP dimensionless units,

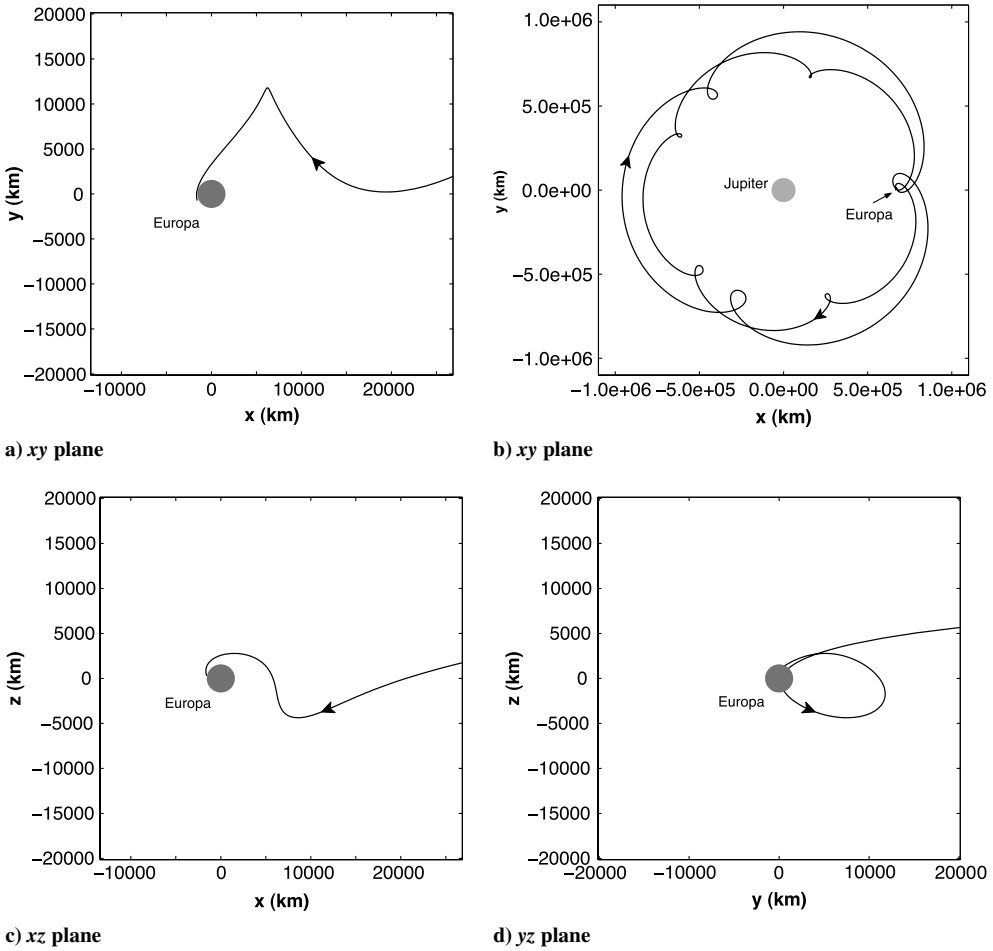

Fig. 4 Projections of the Europa Orbiter baseline trajectory in the Jupiter–Europa rotating frame (including ephemerides). The scale used in these plots is the same as the scale used in Fig. 5, where one dimensionless unit of distance equals approximately 671,039.7 km.

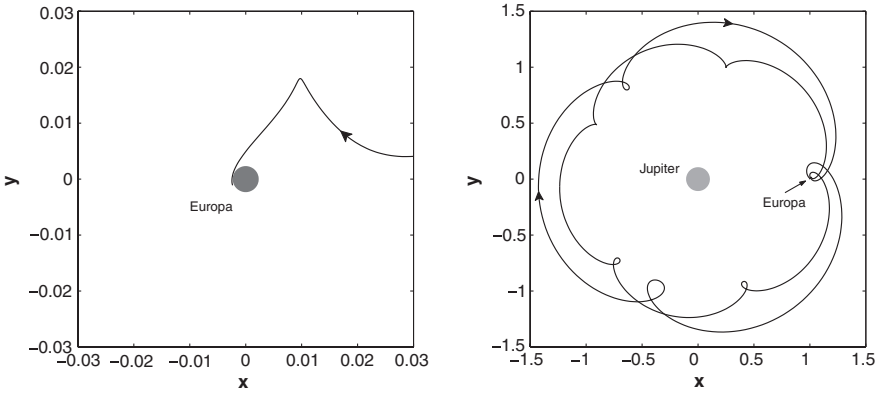

a) *xy* plane b) *xy* plane

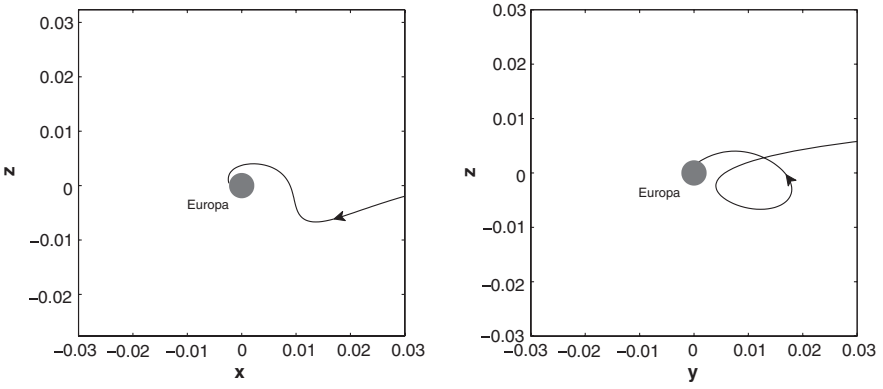

c) *xz* plane d) *yz* plane

Fig. 5 Spatial CRTBP Europa Orbiter trajectory in the Jupiter–Europa rotating frame.

where one dimensionless unit of distance is approximately 671,039.7 km. The μ value used in the CRTBP was approximately 2.526122×10^{-5}. The trajectory retains the same general shape, although the loop shown in the *yz* plane has become a little smaller.

To simplify the problem further and enable the use of a much wider range of techniques, a conversion of the spatial Europa Orbiter trajectory in the CRTBP to a planar trajectory was desired. This conversion was achieved using the differential corrector by constraining the state to remove the z components of the states and specifying a final altitude at Europa. The resulting trajectory is shown in Fig. 6. Most of the trajectory was already nearly planar, so the final result is very similar to the previous plots. The trajectory close to Europa had a significant z component, which is now missing of course, but the trajectory in the *xy* plane looks very similar to the previous trajectories. It is expected that spatial and planar trajectories will both interact with the invariant manifolds of periodic orbits during the approach, but the types of periodic orbits will naturally be different with the removal of the z component. Table 2 shows a comparison of the ΔV magnitudes for each trajectory, although for this study, matching the ΔV magnitudes in each of the models was considered of secondary importance. Therefore, no effort has currently been made to optimize any of the ΔV maneuvers in the new models. As

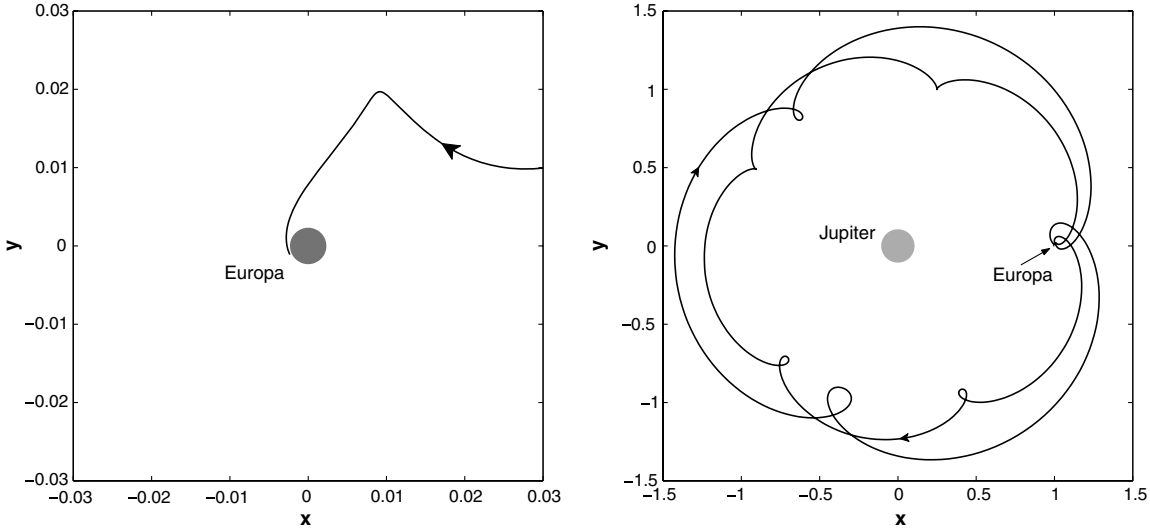

a) *xy* plane (near Europa) b) *xy* plane (entire trajectory)

Fig. 6 PCRTBP Europa Orbiter trajectory in the Jupiter–Europa rotating frame.

Table 2 Comparison of ΔV magnitudes in each model

ΔV	Ephemeris	Spatial CRTBP	PCRTBP
ΔV_1, m/s	118.4	133.5	142.1
ΔV_2, m/s	91.6	150.0	149.7

previously mentioned, this planar trajectory will be the focus of this study.

B. PEO Trajectory in the CRTBP

Figure 7 shows the last portion of the PEO trajectory from the first Europa flyby to EOI in both the inertial and rotating frames. The approximate initial and final positions of this portion of the trajectory are (1.003380, 0.002622) and (0.997628, −0.001111), respectively. From the plot in the inertial frame, it can be seen that there are two primary semimajor axis values, indicating the probable presence of two primary resonances. By examining the two-body period of this trajectory, it can be determined that these are the 3:4 and 5:6 resonances. Visual inspection of the trajectory in the rotating frame using the number of loops on the trajectory can also be used to provide an indication of which resonance the spacecraft is near. The trajectory is also shown in the rotating frame with the location of each ΔV. At each ΔV, the Jacobi constant changes, and the PEO moves to a new energy level. Although the Jacobi constant is not an energy such as that usually calculated in the inertial frame, it is sometimes referred to as the Jacobi energy. That terminology will often be used here.

C. Division of the PEO Trajectory by Energy Levels

Starting at the initial epoch, Fig. 8 shows the osculating two-body period of the PEO trajectory normalized by Europa's period. There are two small jumps in the period that correspond to each ΔV. The large change in period occurs because of the Europa flyby that produces a change in the resonance of the spacecraft. The fluctuations in the period observed at the beginning and end of the time interval as well as during the intermediate Europa flyby correspond to close approaches of Europa, where the two-body calculation of the period with respect to Jupiter is not particularly meaningful. The two maneuvers in this portion of the trajectory were used to divide the trajectory into three segments. The value of the Jacobi constant was then used to differentiate each segment, as indicated in Table 3. It is important to remember that although the Europa flyby appears to change the two-body energy of the spacecraft when the typical two-body approximations are applied, in a three-body sense the Jacobi constant for the spacecraft remains the same before and after the flyby.

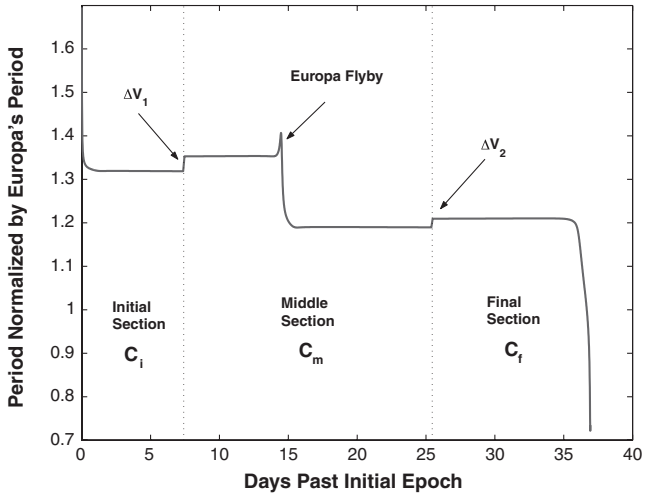

Fig. 8 Normalized two-body period of the PEO over time. The trajectory is divided into sections based on the Jacobi constant, which changes when a ΔV is applied.

D. Unstable Resonant Orbits

Stable resonant orbits are easily calculated using a variety of techniques and can be readily found using Poincaré sections. The calculation of unstable resonant orbits, however, requires some additional effort [11]. The technique currently being used involves the calculation of Poincaré sections with a dense covering of points. Approximate two-body calculations for the period of the resonant orbit are used to select the semimajor axis, and thus L, for the desired orbit. A corresponding point from the Poincaré section closest to the desired value of L with $\bar{g} = 0$ is then chosen. If the corresponding trajectory is sufficiently close to the unstable resonant periodic orbit currently being computed, it may be used as the initial conditions in the single-shooting algorithm. Once the algorithm converges on the desired orbit, trajectories at different energies may be obtained by varying the x-axis crossing of the orbit and reconverging. Plots of some of the points used during this rough continuation process are plotted in Fig. 9. A more detailed continuation analysis is summarized in Anderson [13]. The plots show the value of x used for the initial condition of each resonant orbit versus the Jacobi constant

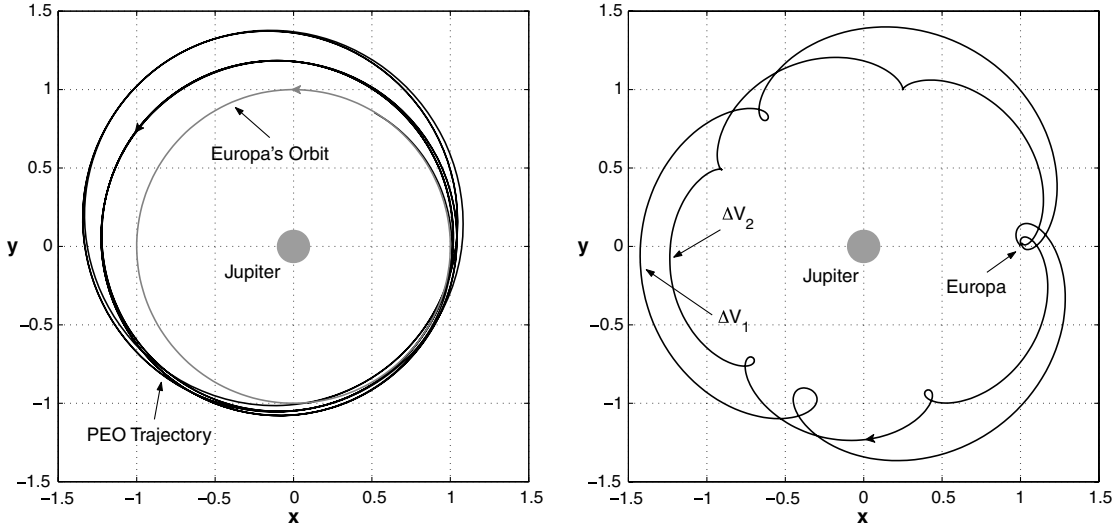

a) Inertial frame **b) Jupiter-Europa rotating frame**

Fig. 7 PEO trajectory from the first Europa flyby to EOI.

Table 3 Jacobi constants for the PEO trajectory in the CRTBP

Segment	Label	Jacobi constant
Initial	C_i	2.98460661333
Middle	C_m	2.99742497175
Final	C_f	3.00245952365

of the converged orbit at this x. The 3:4 and 5:6 unstable resonant orbits analyzed next were computed in this manner.

The 3:4 and 5:6 unstable resonant orbits shown in the rotating frame in Fig. 10 were obtained for the Jacobi constant ($C = C_m$) corresponding to the middle segment of the PEO trajectory. Note that the 3:4 resonant orbit shown here is similar to the 3:4 resonant orbit calculated in the two-body problem in Fig. 1b. Now, however, the

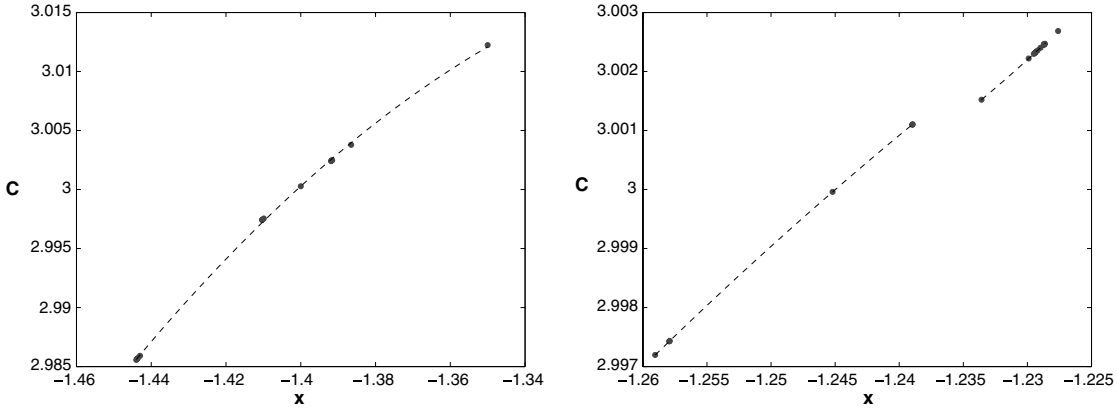

a) 3:4 Resonant orbit **b) 5:6 Resonant orbit**

Fig. 9 Continuation plots for the 3:4 and 5:6 resonant orbits. The points represent the initial conditions on the x axis for each of the converged orbits, and the dashed lines are curve fits through these points. The break in the line in the 5:6 resonant orbit case corresponds to a change in the qualitative nature of the orbit or the existence of two families.

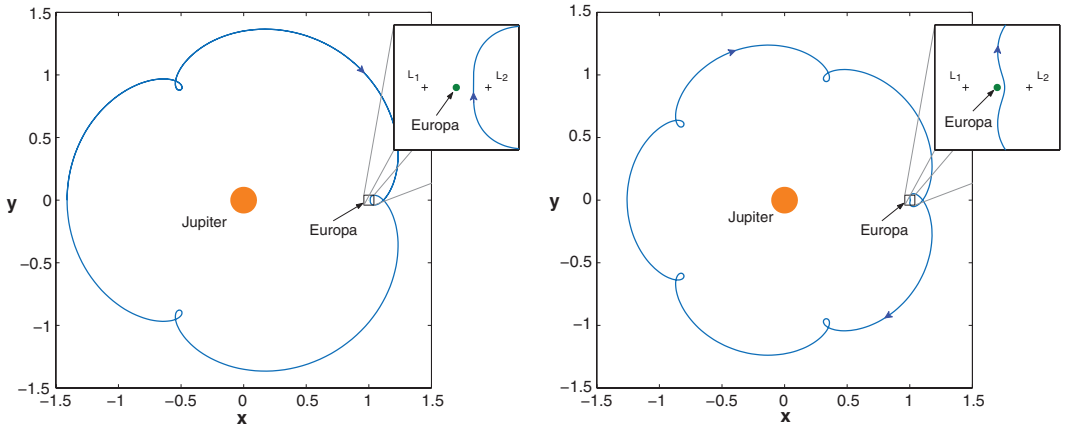

a) 3:4 Resonant orbit **b) 5:6 Resonant orbit**

Fig. 10 Unstable resonant orbits at the middle energy ($C = C_m$). The energy here is greater than at any of the Lagrange points, so the Hill's region does not exist in this planar problem.

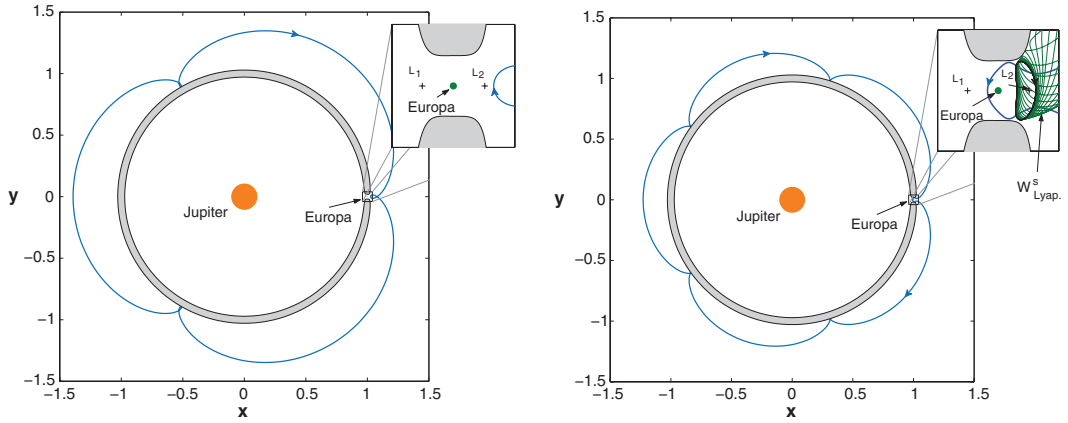

a) 3:4 Resonant orbit **b) 5:6 Resonant orbit**

Fig. 11 The 3:4 and 5:6 unstable resonant orbits at the final energy ($C = C_f$). Note that the 5:6 resonant orbit now passes on the other side of Europa compared to the orbit at $C = C_m$. The gray region is the Hill's region where the spacecraft is forbidden to travel at this energy. The 3:4 resonant orbit shown here was not used by the PEO, but it is shown for comparison with the other resonant orbits.

Table 4 Maximum eigenvalues for monodromy matrix

Segment	Resonance	Maximum eigenvalue
Middle	3:4	270.3
Middle	5:6	1314.7
Final	3:4	86.4
Final	5:6	4441.7

loop near Europa is larger than the others, and the spacecraft no longer returns precisely to its initial conditions in four Europa periods. The 5:6 resonant orbit is even more unusual with a very large loop that changes shape as it travels to the right of Europa. Both of these variations from the trajectories in the two-body problem result from traveling in the nonlinear region near Europa.

The 3:4 and 5:6 resonant orbits in Fig. 11 were computed for the final energy. The 3:4 orbit has a similar shape as the orbit for the middle energy, although the loops are smaller as the orbit has become smaller. The 5:6 resonant orbit at the middle energy now travels on the other side of Europa and goes through a Lyapunov orbit around L_2. This difference indicates that the topological characteristics of the 5:6 resonant orbit have changed, and this new orbit is in a different family. The stability of each orbit was estimated by observing the maximum eigenvalues of the monodromy matrix (the state transition matrix integrated for one period). The 5:6 resonant orbits had larger maximum eigenvalues, as can be seen in Table 4, which indicates that they are more unstable.

E. Resonance Transfer ($C = C_m$)

The use of Poincaré sections most clearly illustrates the mechanics of the resonance transfer that the PEO goes through at the middle energy level. Figure 12 shows such a Poincaré section including the intersection of the resonant orbits and their invariant manifolds compared to the PEO intersections. Note that the invariant manifolds were computed using a parallel supercomputer at JPL, which typically provided an order-of-magnitude improvement in speed compared to using a single processor. The two black points, PEO_1 and PEO_2, in the plot correspond to passes of the PEO trajectory through the x axis at this middle energy. The first pass at this energy (PEO_1) actually occurs, but the second pass (PEO_2) would occur only if the last ΔV were not performed. The point labeled PEO_3 is the actual pass of the PEO through the surface of section after the last ΔV occurs. It is actually at the final energy and is only plotted for comparison with the Poincaré section at the final energy. A Poincaré section showing these points using L and $\bar{g}$ is plotted in Fig. 13. The surface of section on the x axis used for these Poincaré sections is indicated by the black bar in Fig. 14. The black background points show the location of the various resonances relative to the structures of interest. They were computed using a range of initial values for x with $y = 0$, $\dot{x} = 0$, and $\dot{y} = f(C_m)$. The resulting structure possesses several islands surrounded by stable quasi-periodic orbits containing the stable resonant orbits at their centers. Their dynamics are separated from the chaotic sea surrounding the islands, which contains the unstable resonant orbits and corresponding invariant manifolds of interest here. As described in Sec. II.G, the use of relatively small offsets for the invariant manifold computation appears to have produced a faithful representation, and the resulting continuity of the invariant manifolds in the Poincaré sections confirms that the representation is accurate.

The invariant manifolds shown in Fig. 12 have been computed with the focus on the computation of the portions of the manifold near the PEO intersections. What is most striking here is that the invariant manifolds of the 5:6 and 3:4 resonant orbits at this energy are very closely related. As will be observed in the Europa approach discussion, this relationship only exists for particular energies. It is worth noting that the stable manifold W^s of the 5:6 resonant orbit passes very near the 3:4 resonant orbit and its stable manifold near the PEO_1 intersection. It is interesting that the stable manifold of the 5:6 resonant orbit does not extend very far beyond the PEO_1 intersection and curves back on itself. Also, the unstable manifold W^u of the 3:4 resonant orbit passes very close to the 5:6 resonant orbit and its unstable manifold with the PEO_2 intersection lying nearly on top of this manifold. Some gaps appear in this unstable manifold, which might be partly explained by the sparsity of points in general in this area, which can also be observed in Fig. 13. One explanation for this is that these points would have their periapse directly opposite Europa, which appears to be an unstable configuration in this case.

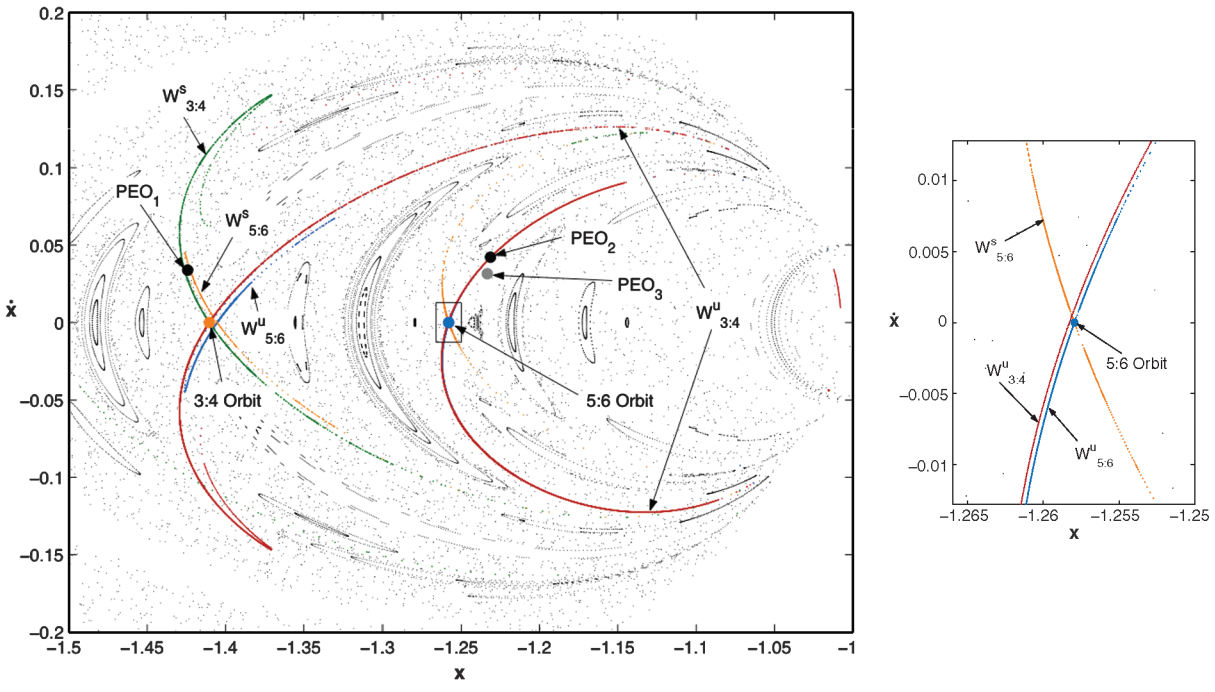

a) Overview including invariant manifolds of each orbit b) Boxed region

Fig. 12 Poincaré section showing mechanics of resonance transfer at $C = C_m$. The unstable resonant orbits are plotted along with their stable (W^s) and unstable (W^u) manifolds. Note that the PEO_2 point would only exist if the last ΔV were not performed. PEO_3 is actually at the C_f energy, but it is plotted for comparison with the Poincaré section at C_f.

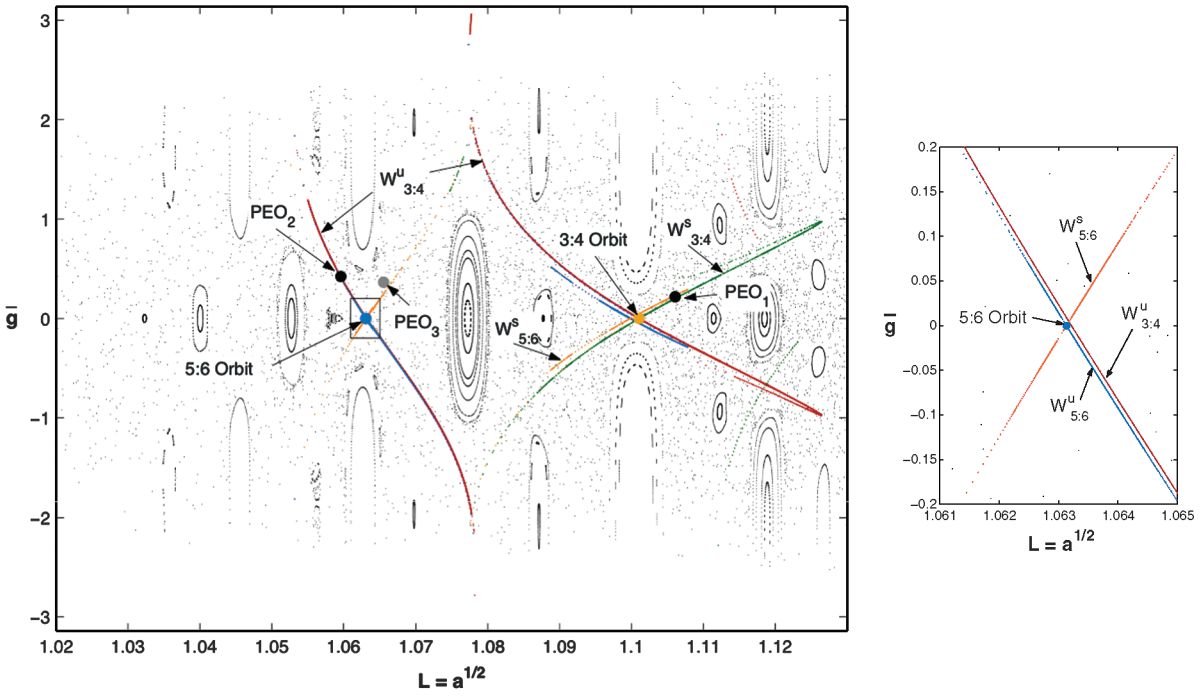

a) Overview including invariant manifolds of each orbit b) Boxed region

Fig. 13 Poincaré section corresponding to Fig. 12 plotted using L and $\bar{g}$. Changes in L more clearly reveal the changes in resonance.

The location of the PEO intersections very near these invariant manifolds indicate that the PEO trajectory is using these manifolds and provides a clue as to how they are used.

This relationship might be even more clearly seen in Fig. 14, in which the trajectories on the stable manifolds of the resonant orbits closest to the PEO_1 intersection and the point on the 3:4 unstable manifold closest to the PEO_2 intersection are plotted with the PEO trajectory at this energy. Looking at the views in Fig. 14b shows that, as observed in the Poincaré section, the PEO initially travels between the stable manifolds in position space. Near Europa, the unstable manifold of the 5:6 resonant orbit also goes between the stable manifolds at which point the PEO approaches it, and follows it, rather than the stable manifolds, away from Europa. In other words, the stable manifolds of the resonant orbits guide the PEO to the unstable manifold of the 3:4 resonant orbit. Taken together, these observations provide the desired mechanism for transition between resonances and give insight into gravity flybys from a three-body perspective. Next, the use of a ΔV sets up the PEO for the final Europa approach.

Before proceeding though, it is interesting to compare these results with the two-body calculations used for flybys. In the two-body

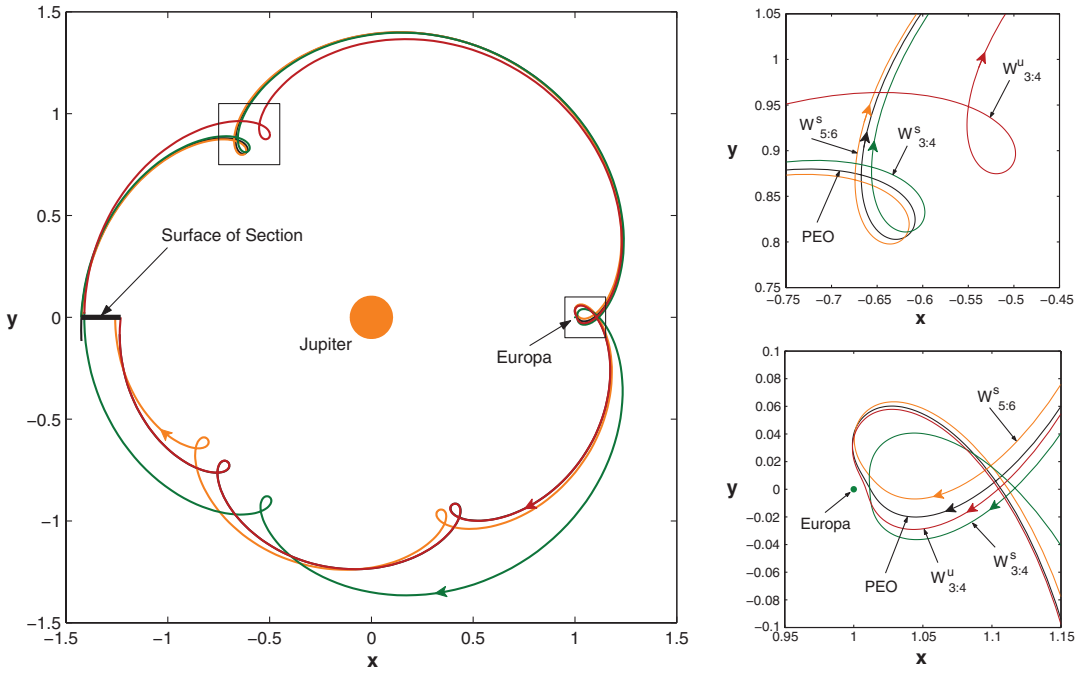

a) Overview of trajectories b) Boxed regions

Fig. 14 Portions of the manifolds of the 3:4 and 5:6 resonant orbits showing how they guide the PEO. The black bar shows the surface of section used in computing the Poincaré section.

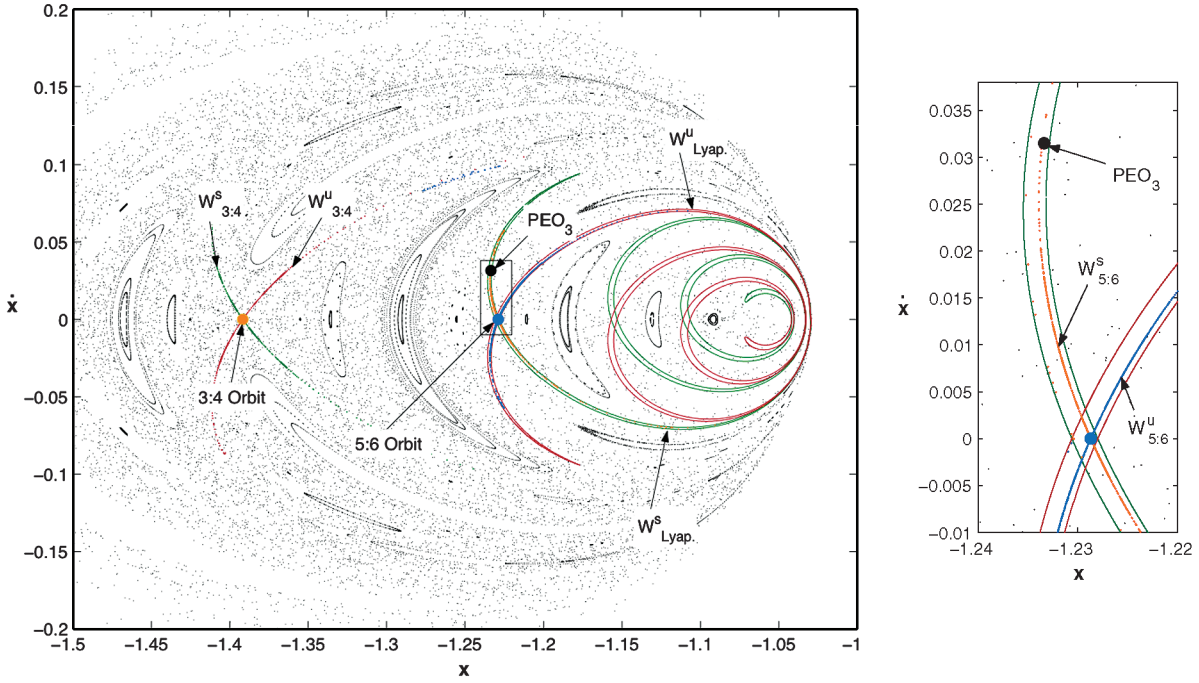

a) Overview including invariant manifolds of each orbit b) Boxed region

Fig. 15 The Europa approach at $C = C_f$. The boxed region on the right gives a closer view of the area near the intersection of the invariant manifolds of the L_2 Lyapunov orbit. The point labeled PEO_3 is the last PEO intersection with the surface of section before insertion. Note that the same color scheme is used here for the invariant manifolds of the 5:6 resonant orbit and the Lyapunov orbit, but they are not related.

calculations, the spacecraft approaches the moon at the sphere of influence with some V_∞. This V_∞ is rotated by the flyby to alter the spacecraft's two-body energy and period, where the resonance is then calculated using the two-body period of the spacecraft compared to the period of Europa. In the three-body approach, the goal is to find the energy where the invariant manifolds of the desired resonant orbits are related in such a way that the spacecraft can use them to travel between the resonances. This approach has several advantages in that it avoids the two-body approximation, and it provides useful geometric artifacts for understanding the dynamics, which can also serve as a design tool. Future work will further explore the potential of this method.

F. Europa Approach and Insertion ($C = C_f$)

The last resonance transition placed the PEO in the area near the 5:6 resonant orbit in the Poincaré section, and a ΔV modified this position slightly. Examining the Poincaré section computed for the

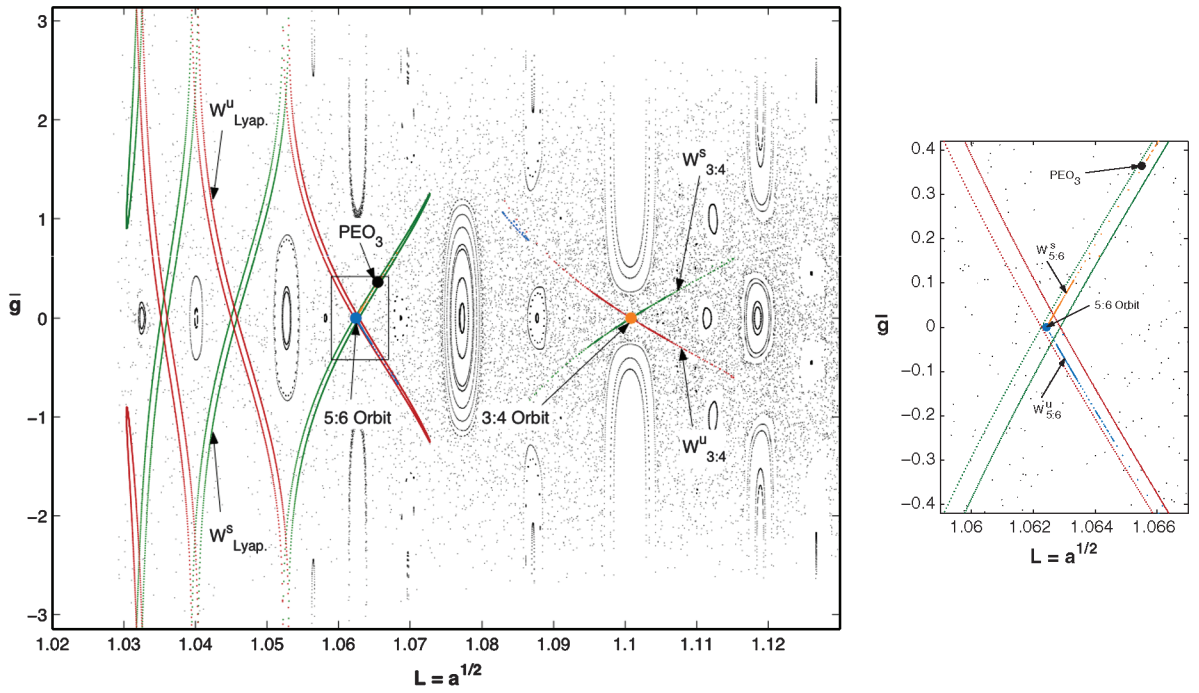

a) Overview including invariant manifolds of each orbit b) Boxed region

Fig. 16 Poincaré section at C_f using L and $\bar{g}$. These variables show the resonance transitions and the various resonances contained within the invariant manifolds of the Lyapunov orbit more clearly.

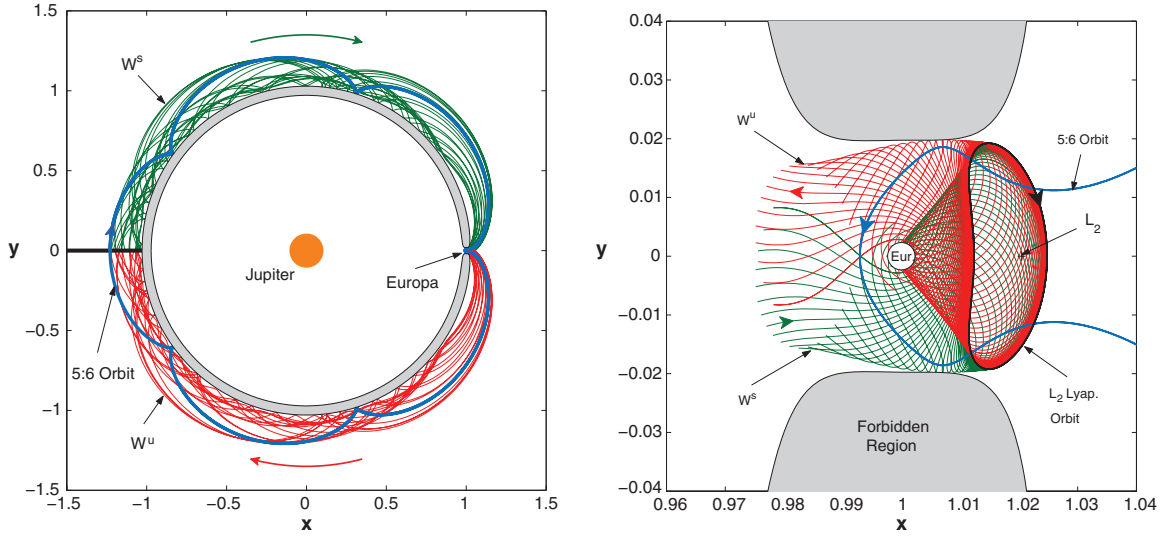

a) Exterior region b) Near Europa

Fig. 17 Set of trajectories on the invariant manifold of the Lyapunov orbit compared to the 5:6 resonant orbit. The invariant manifolds in the exterior region and those near Europa were computed in the opposite sense.

final energy in Fig. 15 reveals the reason for this placement and illustrates the PEO trajectory's use of the stable manifold of an L_2 Lyapunov orbit during the Europa approach. It is interesting that at this energy, the connection between the resonant orbits via the unstable manifolds does not seem to exist. The unstable manifold of the 5:6 resonant orbit approaches the 3:4 resonant orbit as before, but, as can be seen more clearly in Fig. 16, it does not reach the 3:4 resonance. This observation indicates that the resonance transition seen earlier likely only occurs for certain energies.

Here, though, the intersection of the invariant manifolds of the L_2 Lyapunov orbit actually contains the 5:6 resonant orbit. This fact might be expected, since the plot of the 5:6 resonant orbit shows it passing through the L_2 Lyapunov orbit. In addition to this, there appears to be a sequence of resonances where the invariant manifolds also intersect. These resonances can be more clearly seen in Fig. 16, in which the resonance can be determined from L. The intersection of these manifolds provides a region to start searching for these unstable resonant orbits, which is a method currently being used to compute some of these orbits for use in future studies. The fact that the 5:6 resonant orbit lies within the intersection of the invariant manifolds of the Lyapunov orbit, provides the important result that this resonant orbit lives entirely within the invariant manifolds of the Lyapunov orbit for all time. This arises from the fact that the energy surfaces are three-dimensional in this planar problem and therefore possess an inside and an outside. The 5:6 resonant orbit is entirely inside the energy surface formed by the manifolds of the Lyapunov orbit and can not escape. This result is illustrated in Fig. 17, which shows the 5:6 resonant orbit plotted with the invariant manifolds of the Lyapunov orbit. It can be seen that the 5:6 resonant orbit stays within the invariant manifold in position space and moves along the manifold in the external region in Fig. 17a. It is completely within the invariant manifolds as it approaches Europa and the interior region, as can be seen in Fig. 17b. A similar phenomenon has previously been observed for comets that transition between resonances in the exterior and interior regions in the sun–Jupiter system [7]. In addition to this, the relationship between the unstable periodic orbit and the invariant manifolds might allow the computation of such an orbit to be used as a numerical proof of homoclinic orbits that exist at the intersection of the invariant manifolds of the Lyapunov orbit. The fact that there exists a region of significant size within the intersection of the invariant manifolds of the Lyapunov orbit indicates that these unstable periodic orbits persist under small changes in energy. The position of the periodic orbit and the Lyapunov orbit's invariant manifolds will vary continuously with energy, so the periodic orbit

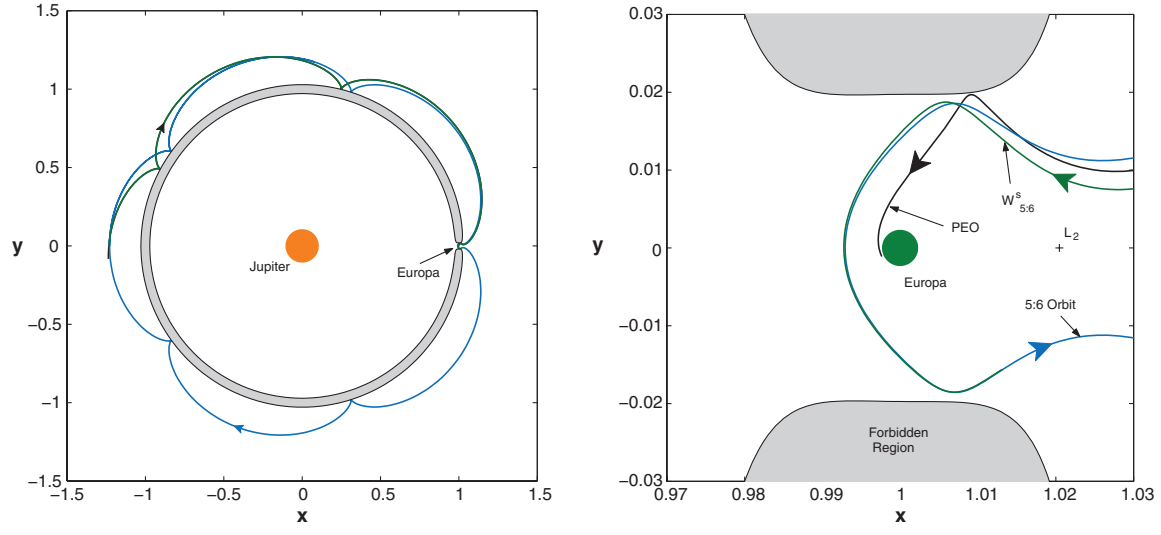

a) Overview of trajectories b) Near Europa

Fig. 18 Comparison of the PEO Europa approach trajectory to a trajectory on the stable manifold of the 5:6 resonant orbit.

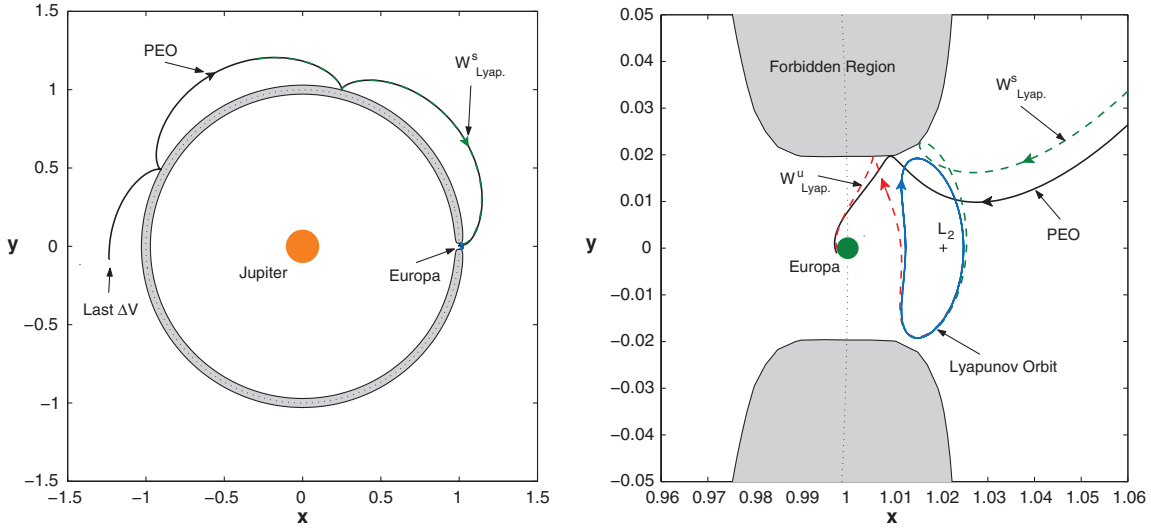

a) Overview of trajectories b) Near Europa

Fig. 19 Europa approach trajectory in the PCRTBP compared to trajectories on the stable and unstable manifolds of the Lyapunov orbit.

family of which this 5:6 resonant orbit is a member will exist within the intersection for a particular range of energies. This correlates to results obtained using the implicit function theorem [29,30] and makes the computation of the orbits practical, since they will exist over a range of energies.

Not only is the 5:6 resonant orbit contained in the intersection of the manifolds of the Lyapunov orbit, but its invariant manifolds shown in Fig. 15b seem to be closely related to those of the Lyapunov orbit as well. The PEO trajectory appears to be using this structure for the Europa approach as its last point in the Poincaré section before capture is contained in the Lyapunov orbit's stable manifold very near to the stable manifold of the 5:6 resonant orbit. This fact indicates it will pass through the L_2 Lyapunov orbit in phase space, as would be expected, near the 5:6 resonant orbit. This result agrees with previous studies that have shown that the Lyapunov orbit acts as a gateway through which all trajectories traveling into the interior region must pass [7,31]. The location of the PEO orbit within the stable manifold of the Lyapunov orbit in Fig. 15b is related to the targeting of the orbit within the Lyapunov orbit's manifold for EOI. What is most interesting here is that the 5:6 resonance is the last in the sequence of resonances contained in the stable manifold of the Lyapunov orbit in Fig. 16. This information indicates that, at least for this energy, a 5:6 resonance is required for the Europa approach and explains why previous trajectory designs have found it necessary to use a 5:6 resonance as the last resonance before Europa approach.

The PEO's use of the stable manifolds of the 5:6 resonant orbit and the Lyapunov orbit can be even more clearly seen by plotting single trajectories on the invariant manifolds to compare with the PEO approach segment. Figure 18 shows the PEO compared to a trajectory on the 5:6 resonant orbit corresponding to the point nearest the PEO intersection in the Poincaré section. In general, the PEO appears to follow this manifold, as shown in Fig. 18a. However, as can be seen in Fig. 18b, the stable manifold approaches the resonant orbit rather than Europa as both trajectories near the vicinity of Europa. It is interesting to note here how Europa appears to perturb the stable manifold onto the resonant orbit over a very short distance. A trajectory on the stable manifold of the Lyapunov orbit is also plotted for comparison with the PEO trajectory in Fig. 19. Here, the PEO generally follows the trajectory on the stable manifold as well as a selected trajectory on the unstable manifold of the Lyapunov orbit. To summarize, the trajectory on the stable manifold of the Lyapunov orbit travels on one side of the PEO and inserts onto the Lyapunov orbit just short of reaching Europa. The trajectory on the stable manifold of the resonant orbit travels on the other side of the PEO and inserts onto the resonant orbit after traveling past Europa. The desired trajectory for a Europa approach would travel between these two trajectories. The PEO does indeed travel between the two and inserts around Europa, which corresponds to the fact that the PEO intersection with the Poincaré section lies between these two manifolds. So it appears that the stable manifolds as seen in the Poincaré section may bound the Europa approach trajectories.

IV. Conclusions

An understanding of resonance transition and approach scenarios for a Galilean moon tour using discrete maneuvers has been gained using dynamical systems techniques. This understanding was achieved by examining the Ganymede-to-Europa portion of the planar Europa trajectory. The analysis has shown that the PEO trajectory closely follows the invariant manifolds of unstable resonant orbits during resonance transition. The PEO uses maneuvers to target desired energies where the invariant manifolds of different resonant orbits are closely related. For the energy level in the PEO scenario, it has been shown that the Europa approach required the spacecraft to reach the 5:6 resonance rather than the 3:4 resonance. This analysis has also demonstrated that the final ΔV gives the PEO the correct state and energy to place it within the stable manifold of the L_2 Lyapunov orbit for the Europa approach and capture.

Although these techniques have been primarily used for analyzing the Europa Orbiter trajectory, several extensions to mission design are apparent. The desired energy for a resonance transition could be determined by computing multiple Poincaré sections over a range of energies and selecting the energy where the invariant manifolds of the relevant unstable orbits are interconnected in such a way as to allow the resonance transitions. Extending this further, a trajectory could then be designed that would connect multiple resonant orbits using their invariant manifolds. This scenario would be analogous to using multiple gravity flybys, but without the approximations of the two-body problem. The final conditions necessary for approach and capture could then be determined using the stable manifold of a Lyapunov orbit. This information would give the resonance required for the approach for a given energy and could aid in selecting the final energy. Currently, these methods should give approximate constraints for trajectory design, and additional work will focus on refining these constraints even further. Finally, the methods developed to handle these phases of the Galilean moon tour provide a solid basis for aiding in the design of similar tours using low thrust.

Acknowledgments

This work was conducted for the Jet Propulsion Laboratory (JPL), California Institute of Technology, under contract with NASA. It was funded in part by the Jupiter Icy Moons Orbiter mission design tool development task. The supercomputer used in this investigation was

provided by funding from JPL Institutional Computing and Information Services and the NASA Offices of Earth Science, Aeronautics, and Space Science. The authors would especially like to thank George Born for his support of the research and Bob Easton for his helpful discussions. Thanks to Jennie Johannesen for providing the Europa Orbiter trajectory, which was the joint work of Jennie Johannesen, Eugene Bonfiglio, and Nathan Strange of JPL as well as Masataka Okutsu and Andrew Heaton of Purdue University.

References

[1] Bollt, E., and Meiss, J. D., "Targeting Chaotic Orbits to the Moon Through Recurrence," *Physics Letters A*, Vol. 204, Aug. 1995, pp. 373–378.
doi:10.1016/0375-9601(95)00502-T

[2] Poincaré, H., *Les Méthodes Nouvelles de la Mécanique Céleste*, Gauthier–Villars, Paris, 1892.

[3] Schroer, C. G., and Ott, E., "Targeting in Hamiltonian Systems That Have Mixed Regular/Chaotic Phase Spaces," *Chaos*, Vol. 7, No. 4, Dec. 1997, pp. 512–519.
doi:10.1063/1.166277

[4] Standish, E. M., "JPL Planetary and Lunar Ephemerides, DE405/LE405," Jet Propulsion Lab., Rept. IOM 312.F- 98-048, Pasadena, CA, 26 Aug. 1998.

[5] Strange, N. J., and Longuski, J. M., "Graphical Method for Gravity-Assist Trajectory Design," *Journal of Spacecraft and Rockets*, Vol. 39, No. 1, Jan.–Feb. 2002, pp. 9–16.
doi:10.2514/2.3800

[6] Okutsu, M., Debban, T. J., and Longuski, J. M., "Tour Design Strategies for the Europa Orbiter Mission," *Advances in the Astronautical Sciences*, Vol. 109, Part III, 2001, pp. 2269–2284.

[7] Koon, W. S., Lo, M. W., Marsden, J. E., and Ross, S. D., "Heteroclinic Connections between Periodic Orbits and Resonance Transitions in Celestial Mechanics," *Chaos*, Vol. 10, No. 2, June 2000, pp. 427–469.
doi:10.1063/1.166509

[8] Howell, K. C., Marchand, B., and Lo, M. W., "Temporary Satellite Capture of Short-Period Jupiter Family Comets from the Perspective of Dynamical Systems," *Journal of the Astronautical Sciences*, Vol. 49, No. 4, Oct.–Dec. 2001, pp. 539–557.

[9] Belbruno, E., and Marsden, B., "Resonance Hopping in Comets," *Astronomical Journal*, Vol. 113, No. 4, 1997, pp. 1433–1444.
doi:10.1086/118359

[10] Lo, M., and Ross, S., "Low Energy Interplanetary Transfers Using Invariant Manifolds of L_1, L_2, and Halo Orbits," *Advances in the Astronautical Sciences*, Vol. 99, Part II, 1998, pp. 551–562.

[11] Lo, M. W., Anderson, R. L., Whiffen, G., and Romans, L., "The Role of Invariant Manifolds in Low Thrust Trajectory Design (Part I)," *Advances in the Astronautical Sciences*, Vol. 119, 2004, pp. 2971–2990.

[12] Anderson, R. L., and Lo, M. W., "The Role of Invariant Manifolds in Low Thrust Trajectory Design (Part II)," AIAA/AAS Astrodynamics Specialist Conference, AIAA Paper 2004-5305, Providence, RI, Aug. 2004.

[13] Anderson, R. L., "Low Thrust Trajectory Design for Resonant Flybys and Captures Using Invariant Manifolds," Ph.D. Thesis, University of Colorado at Boulder, Boulder, CO, 2005.

[14] Lo, M. W., Anderson, R. L., Lam, T., and Whiffen, G., "The Role of Invariant Manifolds in Low Thrust Trajectory Design (Part III)," AAS/AIAA Astrodynamics Specialist Conference, Paper AAS-06-190, Tampa, FL, Jan. 2006.

[15] Johannesen, J. R., and D'Amario, L. A., "Europa Orbiter Mission Trajectory Design," *Advances in the Astronautical Sciences*, Vol. 103, Part III, 1999, pp. 895–908.

[16] Whiffen, G. J., "An Investigation of a Jupiter Galilean Moon Orbiter Trajectory," *Advances in the Astronautical Sciences*, Vol. 116, 2003, pp. 683–702.

[17] Wilson, R. S., "Derivation of Differential Correctors Used in GENESIS Mission Design," Jet Propulsion Lab., Rept. IOM 312.I- 03-002, Pasadena, CA, 2003.

[18] Pernicka, H. J., "The Numerical Determination of Lissajous Orbits in the Circular Restricted Three-Body Problem," M.S. Thesis, Purdue Univ., West Lafayette, IN, Dec. 1986.

[19] Sweetser, T., Maddock, R., Johannesen, J., Bell, J., Penzo, P., Wolf, A., et al., "Trajectory Design for a Europa Orbiter Mission: A Plethora of Astrodynamic Challenges," *Advances in the Astronautical Sciences*, Vol. 95, Part I, 1997, pp. 901–920.

[20] Ludwinski, J. M., Guman, M. D., Johannesen, J. R., Mitchell, R. T., and Staehle, R. L., "The Europa Orbiter Mission Design," *49th International Astronautical Congress*, Paper IAF-98-Q.2.02, Melbourne, Australia, 1998.

[21] Szebehely, V., *Theory of Orbits: The Restricted Problem of Three Bodies*, Academic Press, New York, 1967, pp. 7–41.

[22] Roy, A. E., *Orbital Motion*, 3rd ed., Adam Hilger, Philadelphia, 1988, pp. 111–163.

[23] Murray, C. D., and Dermott, S. F., *Solar System Dynamics*, Cambridge Univ. Press, Cambridge, England, U.K., 1999, pp. 421–428.

[24] Barrabés, E., and Gómez, G., "Three-Dimensional p-q Resonant Orbits Close to Second Species Solution," *Celestial Mechanics and Dynamical Astronomy*, Vol. 85, 2003, pp. 145–174.
doi:10.1023/A:1022098510161

[25] Wiggins, S., *Introduction to Applied Nonlinear Dynamical Systems and Chaos*, 2nd ed., Vol. 2, of Texts in Applied Mathematics, Springer–Verlag, New York, 2003, pp. 28–70.

[26] Howell, K. C., and Breakwell, J. V., "Three-Dimensional, Periodic, 'Halo' Orbits," *Celestial Mechanics*, Vol. 32, No. 1, Jan. 1984, pp. 53–71.
doi:10.1007/BF01358403

[27] Masdemont, J., and Mondelo, J. M., "Notes for the Numerical and Analytical Techniques Lectures (Draft Version)," *Advanced Topics in Astrodynamics Summer Course*, Barcelona, July 2004, http://www.ieec.fcr.es/astro04/notes/analnum.pdf [retrieved 2010].

[28] Parker, T., and Chua, L. O., *Practical Numerical Algorithms for Chaotic Systems*, Springer–Verlag, New York, 1989, pp. 130–166.

[29] Meyer, K. R., and Hall, G. R., *Introduction to Hamiltonian Dynamical Systems and the N-Body Problem*, Springer–Verlag, New York, 1992, pp. 109–167.

[30] Hénon, M., "Numerical Exploration of the Restricted Problem, V," *Astronomy and Astrophysics*, Vol. 1, Feb. 1969, pp. 223–238.

[31] Conley, C., "Low Energy Transit Orbits in the Restricted Three-Body Problem," *SIAM Journal on Applied Mathematics*, Vol. 16, 1968, pp. 732–746.
doi:10.1137/0116060